POLITECNICO DI TORINO
Repository ISTITUZIONALE

Model-based design of secondary drying using in-line near-infrared spectroscopy data

(Article begins on next page)

18 April 2024

Model-based Design of Secondary Drying using in-line Near-Infrared Spectroscopy Data

Serena Bobba[1,2], Nunzio Zinfollino[2], Davide Fissore[1]

1. Dipartimento di Scienza Applicata e Tecnologia, Politecnico di Torino, corso Duca degli Abruzzi 24, 10129 Torino

2. Biotech Pharmaceutical Development Department, Merck Serono SpA, via Luigi Einaudi 11, 00012 Guidonia Montecelio (Roma)

Abstract

This paper deals with the design and optimization of the secondary drying stage, via design space calculation, of a freeze-drying process. A simple and well known mathematical model was used to this purpose: the kinetic parameters of the water desorption step were determined, either off-line or in-line, using the measurement of the residual amount of water (C_s) in one of the processed samples through Near-Infrared spectroscopy. In the first approach, three tests, at different values of heating shelf temperature, are employed: the measurement of C_s vs. time allows estimating the desorption rate and, finally, the kinetic constant at the given temperature. Arrhenius plot is used to get the parameters expressing the dependance of the kinetic constant on product temperature, thus allowing the calculation of the design space. In the second approach, the kinetic parameters are estimated in-line, focusing on the first part of the secondary drying stage, where the variation of product temperature is more relevant, hence allowing to track the evolution of the desorption rate (via C_s measurement) vs. product temperature. A fitting procedure is then used, looking for the kinetic parameters that provide the best fit between calculated and measured values of C_s. By this way only one test is required to get the design space. Drying of sucrose and of sucrose – arginine mixtures were used as case studies, to point out the effectiveness of the proposed method. Examples of the design spaces that can be obtained are presented and discussed, focusing on the effect of operating parameters like the heating rate and the residual water content at the beginning of the secondary drying, as well as on the constraint about the maximum allowed temperature.

Keywords

List of Abbreviations

KF	Karl-Fischer
MVA	Multivariate Analysis
NIR	Near-Infrared
NIRS	Near-Infrared Spectroscopy
PAT	Process Analytical Technology
PLS	Partial Least Square
PRT	Pressure Rise Test
RM	Residual Moisture
RMSE	Root Mean Squared Error

List of Symbols

A_v — cross-sectional area of the vial, m^2

a — specific surface of the product, $m^2\,kg^{-1}$

C_s — water content, % (w/w)

$C_{s,eq}$ — residual moisture at the end of secondary drying, % (w/w)

$C_{s,t}$ — target residual moisture, % (w/w)

$C_{s,0}$ — water content at the beginning of secondary drying, % (w/w)

c_p — specific heat, $J\,kg^{-1}\,K^{-1}$

E_a — energy of activation of the desorption reaction, $J\,mol^{-1}$

ΔH_d — heat of desorption of water, $J\,kg^{-1}$

K — ratio of free volumes

K_v — effective heat transfer coefficient, $W\,m^{-2}\,K^{-1}$

k_d — kinetic constant of the desorption rate, $kg\,m^{-2}\,s^{-1}$

k_0 — pre-exponential factor of the desorption rate, $kg\,m^{-2}\,s^{-1}$

R — ideal gas constant, $J\,mol^{-1}\,K^{-1}$

r_d — water desorption rate, % (w/w) s^{-1}

T_f — temperature of the heating fluid, K

$T_{f,max}$ — maximum fluid temperature, K

T_g — glass transition temperature, K

$T_{g,s}$ — glass transition temperature of solute, K

$T_{g,w}$ glass transition temperature of water, K

T_p product temperature, K

t_d drying time, h

V volume of the cake, m^3

Greeks

ρ density, kg m^{-3}

ρ_s density of solute, kg m^{-3}

ρ_w density of water, kg m^{-3}

1. Introduction

In the last decades, especially after the Food and Drug Administration's PAT initiative of 2004[1], Quality-by-Design has become a fundamental strategy in the pharmaceutical field, in order to get high quality products and highly efficient processes. The process efficiency is of outmost importance for freeze-drying, to shorten the duration and, thus, reduce costs. Freeze-drying is an essential step in the manufacturing of (bio)pharmaceuticals[2], as it allows to preserve the active component characteristics by means of a gentle drying process. Hence, despite of the fact that the entire cycle may last several days, it is vastly used for drying heat-sensitive products.

A freeze-drying cycle is basically made up of by three steps. Firstly, during the freezing, the product temperature is lowered and most of the liquid solvent (generally water) is turned into ice, except for a fraction of water that remains incorporated in the product. Following, in the primary drying step, the product temperature is maintained low, and the chamber pressure is decreased to allow the sublimation of ice crystals. As the water content at the end of primary drying is usually too high, because of the unfrozen water that cannot sublimate, secondary drying, the last step, is performed. Temperature is increased while pressure is kept at low values, and the desorption of the unfrozen water from the product occurs as the aim is achieving the target residual moisture (RM), which may be even lower than 1%[3].

Primary drying is typically the most time-consuming phase of the cycle and great attention has to be paid in this step to avoid the overheating of the product and the collapse of the cake. For this reason, numbers of studies were done in order to develop methods for design and monitoring this stage. Hence, primary drying is nowadays well understood: methods to identify the end-point[4,5,6], 2D models[7-10], and algorithms to calculate a design space[11,12] were proposed and are now available to industrial practitioners. Comparatively, a little work was done about designing the secondary drying. Some accurate models were proposed to simulate the primary and secondary drying steps[13,14], though the calculations involved required the use of a lot of parameters. Nevertheless, the secondary drying step would deserve serious consideration. In fact, it may be as time consuming as the primary drying, and it may account for at least 20% of the operational costs[15]. Additionally, meeting the target RM is essential: firstly, the over-drying of the product has to be avoided, as it can damage the active component; on the opposite, a higher RM is not desirable, as it would affect the shelf-life stability.

When it comes to process development, a simple method to estimate the end-point of the secondary drying is by means of a trial-and-error approach: some samples are taken periodically

from the chamber using a sample-thief, through a special flange in the chamber door, without interrupting the cycle. Their RM is obtained typically by means of Karl Fischer (KF) titration, and, thus, the ending point of secondary drying is established according to the target RM. However, handling the samples with a sample-thief is challenging and the accuracy of the method depends on the sampling frequency, that is limited being the method destructive. Moreover, if the operating temperature has to be optimized, these tests have to be repeated in several cycles where the heating temperature is changed. Finally, this procedure is not complying with the Quality-by-Design approach: the PAT initiative[1] suggests to develop and design processes continuously controlled, to ensure higher product quality, by means of well understood and efficient processes. In fact, to deal with the PAT guideline, the implementation of PAT (Process Analytical Technology) tools is necessary. These tools are process and product analyzers, that provide information in-line and in real-time about the status of the product and of the process[16]. PAT tools have been implemented for monitoring batch freeze-drying for pharmaceuticals, aiming at in-line or off-line process optimization[17]. The information collected can be used to build a design space. The design space includes the combinations of process variables and parameters that guarantee a final product in compliance with the quality targets[18], according to the Quality-by-Design concept.

Studies about the secondary drying focused on the investigation of the desorption kinetics[19,20] and on the impact of process parameters[21-23] on it, e.g. temperature and chamber pressure. The methods proposed were aimed at setting the operating conditions for this stage, but could not predict the RM content[24], or, conversely, could predict the RM, but required a considerable experimental work[25]. Strategies for in-line monitoring of secondary drying and detecting the end-point were presented, based on tunable diode laser absorption spectroscopy[26] or on Pressure Rise Test (PRT)[19,27,28]. In this framework, Near-Infrared Spectroscopy (NIR spectroscopy or NIRS) can be a powerful tool to be installed in-line and used as a PAT tool. NIR technology is a non-invasive spectroscopic technique, based on the measurement of the absorbance of the system in the range 14300-4000 cm^{-1} (700-2500 nm)[29-33]. In particular, NIRS is able to detect water with high accuracy, since water gives strong signals around 6900 cm^{-1} and 5150 cm^{-1} [34]. This characteristic makes NIRS particularly suitable for evaluating the RM of freeze-dried products. Indeed, this technique was exploited in several studies for freeze-drying applications, both as an off-line analyzer for the measurement of RM, active component, and cake structure[35-39], and for in-line monitoring of the water content and of the modifications of proteins structures[16,40-43]. In particular, some applications for studying the water dynamics during the secondary drying were presented, proving the suitability of NIRS for detecting water

even when the concentration is very low[44,45].

In this study NIRS was used as an in-line tool to get a real-time measurement of the water content of the product being freeze-dried. Spectra of a sample being freeze-dried were collected during the entire cycle, and a model for RM prediction was developed from spectral data, by Partial Least Square (PLS) regression[29,31,46-48]. Following, the trend of water content during the secondary drying was used to calculate the desorption rate and, finally, the kinetic constant of the process. This allowed to use a simple model of the secondary drying stage to calculate the design space, i.e. the range of operating conditions, namely the temperature of the heating fluid and the drying time, to reach the target RM avoiding the product over-heating and, lately, meeting the PAT guidelines about Quality-by-Design.

The temperature dependence of the desorption kinetic is usually assumed to be of Arrhenius-type[7,28], hence two parameters, namely the energy of activation of the desorption reaction (E_a) and the pre-exponential factor (k_0) have to be estimated. In this work two methods are proposed to estimate these parameters:

(i)   the first is based on the off-line calculation of the Arrhenius plot, using the method of Pisano et al.[28], but without using the PRT, and taking advantage of the measurements of water content through NIRS;

(ii)   the second is a completely new approach, based on the in-line fitting of the measures of water content with the secondary drying model.

While the first approach requires carrying out three tests, at three different temperatures, in the second one just a single test may be enough. Moreover, method (i) requires carrying out the tests till the completion of the secondary drying, and, thus, it may be used only off-line. Conversely method (ii) uses the measurement of water content in the first part of the secondary drying stage, where product temperature changes. This would be very beneficial to calculate the kinetic parameters and, thus, the design space, in-line, allowing a real-time process control and optimization. It has to be remarked that in this work only the effect of temperature was considered for designing the secondary drying, since it was already proved that pressure had a negligible effect on the desorption kinetics[21].

This paper is organized as follows: in section 2 the NIRS model for RM prediction, the model equations and the algorithm used for the calculation of the design space are presented, as well as the experimental setup; section 3 shows the results regarding the estimation of the kinetic parameters for two different products, and an example of a design space calculated when some process conditions are varied; section 4 highlights remarkable conclusions.

2. Methods and Materials

2.1 Experimental procedure and case study

Experimental activities were carried out in the laboratories of the Guidonia Montecelio (Italy) site of Merck Serono SpA. As case studies for developing and testing the proposed algorithms two products were used:

– product A: sucrose 6% (w/w);

– product B: sucrose 6% (w/w) and arginine 2% (w/w) (total solid fraction 8% w/w).

These samples were obtained from aqueous solutions, freeze-dried in vial 2R (Nuova Ompi, Piombino Dese, Italy), with a filling volume of 1 mL. Sucrose and L-arginine monohydrochloride were supplied by Merck Life Science (Darmstadt, Germany), and used as received, while ultra-pure water was obtained by a Millipore water purification system (IQ 7000, Merck Millipore, Burlington, USA). Vials were placed in direct contact with the freeze-drier shelf, in a honeycomb layout, using a polymeric square frame. This was specifically designed for in-line NIRS monitoring (Figure S1 in Supplementary material): a carving on one of the sides of the frame was realized to allow NIRS probe to be placed in direct contact with the vial to be analyzed in-line.

For spectra acquisition a Fourier Transform NIR spectrometer (Antaris MX FT-NIR, Thermo Fischer Scientific, Waltham, USA), equipped with a halogen NIR source and an InGaAs detector, was used. Spectra were recorded in diffuse reflectance mode, in the wavelength range 10000 - 4000 cm^{-1}, with the following setting: 32 scans, resolution of 8 cm^{-1}, gain of 1, and 3 minutes is the time interval of acquisition. The NIRS probe was installed in-line, through a specifically designed flange of the freeze-dryer door. The probe was placed in contact with the monitored sample, that was the vial in the middle of the first raw in the frame (Figure S1 in Supplementary material). Therefore, the position of the samples analyzed in-line with respect to the freeze-dryer chamber was always the same. This was relevant to eliminate any potential effect due to the positioning of the product on the shelf, as the thermal evolution of a vial may be strongly affected by vial position[49,50]. Actually, a single vial could be monitored at a time, since a single NIR probe could be installed through the freeze-drier door. Previous tests evidenced that both temperature and overall heat transfer coefficient in the monitored vial, in this arrangement, are included in the range of variability of these parameters in the central vials of the batch, those constituting the majority of the batch.

Product temperature was monitored in-line by wireless sensors (Tempris GmbH, Holzkirchen, Germany). Three sensors were used for each run, placed in the vials just beside and in contact with the vial monitored by NIRS.

Samples were processed in a lab-scale freeze-drier (Lyostar3, SP Scientific, Warminster, USA). Samples of type A and B underwent to different process conditions during the secondary drying, in order to study the desorption kinetics as a function of temperature, while freezing and primary drying were kept unchanged for all the batches.

Three cycles were initially performed for samples A (Figure S2 in Supplementary material, with the following process conditions:

- freezing up to -45°C, with an annealing step of 2 h at -15°C, for a total time of 8 h;
- primary drying at -23°C and 5 Pa for 30 h;
- secondary dying at 20, 30, and 40°C (a different temperature setpoint was used for each cycle) and 5 Pa for 40 h. These runs are called in the following A1, A2, and A3, referring to the drying temperature at 20, 30, 40°C respectively.

A further cycle, called A4, was run with product A (Figure S3 in Supplementary material , with the same freezing protocol and the following settings for drying:

- primary drying at -25°C and 5 Pa for about 59 h;
- secondary drying at 35°C and 5 Pa for about 19 h, with a slower heating rate set at +0.1°C/min.

This test was carried out to validate the kinetic model developed off-line using the results of the previous tests.

Samples B were obtained from two cycles (Figure S4 in Supplementary material):

- freezing at -45°C, with an annealing step of 2 h at -15°C, for a total time of 8 h;
- primary drying at -25°C and 5 Pa for 34 h;
- secondary dying at 20 and 45°C (a different temperature setpoint for each cycle) and 5 Pa for 40 h. In the following these runs are called B1 and B2, identifying respectively the run at 45°C and 20°C.

Just one of this two tests (B1) was used to estimate the kinetic parameters for the desorption reaction, while the other (B2) was needed to validate the model developed with the first one. When not specified, the cooling/heating rate of the cycles was set at +/- 1°C/min.

2.2 Water content measurement

For developing a NIRS application, typically a large number of spectra needs to be collected, and each spectrum is made by hundreds of values (one for each wavelength scanned). As a

consequence, Multivariate Analysis (MVA) is needed to process NIRS data and extract any relevant information. Among the MVA methods, PLS was adopted in this study to get a prediction of the RM content.

Samples of sucrose 6% w/w and of sucrose 6% w/w - arginine 2% w/w were freeze-dried and humidified, following the procedure proposed in literature[51]. These samples were scanned by NIRS, and KF titration was used as the reference analytical method for calibrating the PLS regression. Data were processed according to the method described by Bobba et al.[46]. This method was intended to calibrate a robust model. Two different models for estimating the RM from NIRS spectra, were developed, one for product A and the other for product B. The approach is based on the use of a small wavelength range (5290 - 4785 cm^{-1} for samples A, and 5295 - 4745 cm^{-1} for samples B), very specific for the water signal, in order not to consider other product-specific signals, and just two latent variables were used to perform the modeling. The models were validated off-line with other samples of the tested product, in the range of RM 0.36% - 6.35% for samples A, and 0.30% - 3.84% for samples B. The validation resulted in very low estimated errors, i.e. the Root Mean Square Error of Prediction and the Root Mean Square Error of Cross Validation respectively equal to 0.123 and 0.122, meaning that the model could be considered pretty much accurate.

This model was also applied to the spectra collected in-line, resulting in the prediction of the water content of the sample undergoing freeze-drying. Because of the range of RM used for the calibration, the model could predict the water content reliably only in the last part of primary drying, in particular in the holding step after the completion of ice sublimation, and during the entire secondary drying stage. The trends of the water content over the secondary drying in the various tests are showed in Figure S2, S3, and S4 in Supplementary material.

At the end of each run, the RM of the vial monitored by NIRS was assessed by KF titration, as a further validation of the predictive ability of the PLS model (Table 1). When the values of RM measured and predicted are compared, the large uncertainty related to the KF analytical method should be taken into consideration (up to $\pm$ 0.3% w/w)[52,53], which is less accurate than the performance of the NIRS model[45].

2.3 Mathematical modeling

The goal of the mathematical model of the secondary drying is to describe the evolution of the product temperature (T_p) and of the water content (C_s) vs. time. A lumped model is here adopted[28], since radial and axial gradients of temperature may be assumed negligible. Therefore, the energy and mass balance for the product being dried in the vial, i.e. the cake, are

given by equations (1) and (2):

$$\rho c_p V \frac{dT_P}{dt} = K_v A_v (T_f - T_P) + V \rho \, r_d \, \Delta H_d \tag{1}$$

$$r_d = -\frac{dC_s}{dt} \tag{2}$$

where ρ and c_p are the density and the specific heat of the product, V the volume of the cake, A_v the cross-sectional area of the vial, T_f the temperature of the heating fluid, and ΔH_d the heat of desorption of water. The parameters K_v is an effective heat transfer coefficient, taking into account the overall heat transfer mechanisms from the freeze-drier chamber to the product, e.g. conduction through the contact points between the vial bottom and the shelf, conduction in the gas between the vial bottom and the shelf, radiation from the chamber[9,12,54,55]. The water desorption rate (r_d) is defined by equation (3), based on the assumption that the rate-determining step for secondary drying is water desorption from the solid porous cake. In fact, Pikal et al.[21] showed that the vapor transport, i.e. the diffusion, through the dried cake was not rate limiting.

$$r_d = a k_d (C_s - C_{s,eq}) \tag{3}$$

where a is the specific surface of the product[7], k_d the kinetic constant and $C_{s,eq}$ the minimum RM at the end of an extended secondary drying. Equation (3) assumes that r_d is proportional to the difference between the water content and its equilibrium value and, therefore, this is the actual driving force of the desorption phenomena. The value of $C_{s,eq}$ can be eventually equal to zero depending on the product characteristics. This model was demonstrated to describe the physical phenomenon properly[13] and was verified experimentally. The kinetic constant k_d exhibits an Arrhenius-type dependence from the product temperature[28,56,57], as described in equation (4):

$$k_d = k_0 \exp\left(-\frac{E_a}{R \, T_P}\right) \tag{4}$$

where k_0 and E_a are the kinetic parameters named above and R is the ideal gas constant. Additionally, the effect of chamber pressure on the desorption kinetic was assumed negligible[21], at least in the range of pressure values typically used for freeze-drying

applications.

2.4 Estimation of model parameters

In order to solve the system of equations (1) and (2) the physical properties of the product should be known, and some parameters have to be estimated.

The value of the overall heat transfer coefficient is mainly a function of the chamber pressure and it is specific for the vial-chamber system. The method based on gravimetric tests can be used to experimentally estimate its value[55]. Usually, the value of K_v should be already known from previous primary drying design. Indeed, when it comes to secondary drying, the primary drying is supposed to be already designed, and to do this, K_v is an essential parameter. Actually, this was the case: the value of K_v was known as a function of pressure for that specific vial-chamber system, thanks to previous studies. Three gravimetric tests had been performed at 5, 10, 15 Pa using 2R format vial, resulting in K_v values ranging between 15 and 33 W m^{-2} K^{-1} accordingly to the position of the vial across the shelf. In particular, the values of K_v concerning the test run at 5 Pa, i.e. the pressure that was used in the present work to run the cycles used for model developing, ranged between 15 and 23 W m^{-2} K^{-1} according to the position of the vials on the shelf, being the higher values characteristic of vials in the first row of the shelf. However, with the aim to verify the value of K_v for the vial monitored by NIRS, in that specific position on the shelf, was similar to that of central vials, representing the majority of the batch, a single gravimetric test was lead at 5 Pa: the K_v resulted to be 25 W K^{-1}m^{-2} for the vial monitored by NIRS, thus comparable with the value found previously for the edge vials. Also, the values of K_v of the edge vials found from the gravimetric test lead with the NIRS installed inline was equal to about 25 W m^{-2} K^{-1}, thus almost equal to the K_v of the vial monitored by NIRS. This could be another evidence that the NIRS radiation had a minimal effect on the heat exchange of the vial, at least with the equipment, experimental set up, and time interval of spectra collection adopted in this work. This makes the heating effect due to the NIR beam radiation not so significant, as the overall heat transfer appeared not significantly affected.

The value of $C_{s,eq}$ can be evaluated experimentally or calculated from literature correlations, that are estimated empirically for a specific formulation[58,59]. In this case, to get $C_{s,eq}$ values, some preliminary runs were performed at different process conditions, for the products A and B. The $C_{s,eq}$ values found and used in the calculations are summarized in Table 1. They were obtained running secondary drying for about 30 h, which is a time duration definitely much longer than the necessary, since the trend of C_s reached a clearly defined plateau.

The water content at the beginning of secondary drying ($C_{s,0}$) is provided by NIRS in-line

measurements, as well as the C_s at each time step considered in the calculation.

Aiming to compare the results obtained in the three tests carried out at different temperatures, the evolution of C_s versus time cannot be considered, as the value of C_s at the beginning of secondary drying ($C_{s,0}$) could be different from a batch to another. In fact, the end-point of the primary drying might have occurred at different times, thus the water desorption that could have taken place during the holding time in the last hours of primary drying may be different. This might have caused different $C_{s,0}$ between different batches. Therefore, to remove the influence of $C_{s,0}$, the comparison was performed with the normalized trends of water content, i.e. each value of residual water was divided by the value at time zero. Figure 1 (above) shows the comparison between the normalized trends of RM for the three runs required when using method #1. Here, the effect of temperature on the kinetics and on $C_{s,eq}$ can be appreciated. The higher the product temperature, the faster is the decrease of C_s, and the lower the value of $C_{s,eq}$, which turned out in a lower RM content, hence, the dependency of the desorption kinetics on the temperature is confirmed.

The kinetic parameters E_a and k_0a have to be estimated. Two algorithms were proposed to estimate E_a and k_0a as described in the following sections. This kinetic parameters were used to model the evolution of C_s. In order evaluate the goodness of the fitting and compare the performance of the two algorithms, the Root Mean Squared Error (RMSE) was calculated. RMSE was obtained as the root mean squared error of the residuals, i.e. of the difference between the experimental values of C_s and the calculated ones, at the power of two, divided by the number of measurements,.

2.4.1   Arrhenius plot based calculation (method #1)

Similarly to the algorithm proposed in literature[28], this method is focused on the construction of an Arrhenius plot, which takes advantage of the Arrhenius-dependence of k_d from temperature.

Pisano et al.[28] applied the PRT to calculate r_d from measured values of pressure rise in the secondary drying stage. Following, $C_{s,0}$ and k_d were obtained from the fitting of the drying rate measured by PRT in the secondary drying stage. In this study, the implementation of in-line NIRS analysis allowed to get easily the trend of C_s and of $C_{s,0}$, that can be used to calculate the r_d, and following to estimate the value of k_d as shown in the following.

When using this approach it has to be taken into account that product temperature is changing at the beginning of the secondary drying and, thus, aiming to indicate one point in the Arrhenius plot, i.e. a value of k_d for a specific value of product temperature, the attention has to be focused

on the portion of the secondary drying stage where an almost steady state value of product temperature was obtained. Great care has to be paid when selected the values of C_s to be used in the previously described algorithm as not only product temperature has to be reached an almost steady-state value, but also a "relevant" decrease of the water content has to be detected, to allow calculating the desorption rate. This means that data obtained in the last part of the secondary drying, where C_s has reached an almost steady-state value, are useless to calculate the desorption rate. The selection of the optimal window for data extraction may be easily done off-line, once the curve C_s vs. time has been obtained. The algorithm proposed is thus the following:

1. For a given set of operating condition, C_s vs. time was measured through the NIR spectra collected in-line, by applying the PLS regression model;
2. Mathematical manipulations, i.e. smoothing and filtering, of this curve were performed, in order to reduce the measurement noise. Filtering was performed by the MATLAB function *spline*, which consisted in a cubic spline interpolation of data. For smoothing another MATLAB function was applied, *sgolay*, which allowed to design a Savitzky-Golay polynomial filter;
3. Data collected when product temperature was almost constant and the decrease of C_s still significant were selected;
4. The value of the drying rate was calculated from the mass balance, as the ratio between the difference of two subsequent values of C_s and the time interval between them. Because of the filtering algorithm applied to reduce the noise affecting C_s, the time interval between two subsequent values was 6 minutes. Since r_d is obtained as the derivative of C_s vs time, the trend calculated was still quite noisy. Thus, further smoothing was applied to get a smoother trend or r_d.
5. The values of r_d were plotted against the values of C_s -$C_{s,eq}$;
6. A linear fitting of the r_d values vs. C_s -$C_{s,eq}$ allowed to obtain the value of the kinetic constant ($k_d a$), taking into account equation (3).

This procedure has to be performed for at least two tests, run at different temperature conditions. Nevertheless, aiming to improve the accuracy of the method, three tests are here suggested as minimum. In fact, this allows checking if the Arrhenius plot is truly linear. Once the three values of $k_d a$ were obtained, they could be represented in an Arrhenius plot, by applying equation (4) in the logarithmic form. Finally, the values of E_a and $k_0 a$ can be obtained respectively from the

slope and the intercept of the linear fitting of these three points.

This approach was applied to runs A1, A2, and A3, thus, estimating E_a and $k_0 a$ for sucrose 6% w/w. The values estimated were used to calculate the trend of C_s by means of equations (2) and (4), over the entire duration of secondary drying. The validation was performed by comparing the calculated trend of C_s with the trend obtained experimentally from NIRS, as the transitory and final parts of the experimental trend were not used for extrapolating the kinetic parameters. Also run A4, carried out with different operating conditions, was used for validation purposes. As an alternative, a different approach may be used, based on the fact that equations (2) and (3) at constant temperature have an analytical solution describing the evolution of C_s vs. time, and a non-linear fitting algorithm could be used to get the kinetic parameter $k_d a$. In this study we preferred the first approach as it is based on a simpler linear fitting.

2.4.2 Fitting-based calculation (method #2)

An innovative solution to obtain E_a and $k_0 a$ directly from just one test, in-line, is based on the best fitting of the trend of C_s using the previously presented mathematical model where the only unknown parameters are E_a and $k_0 a$. The fitting procedure was performed by MATLAB functions, implemented in some scripts written ad-hoc.

Since, from the experimental trends (Figure S2 and S3 in Supplementary material), the most significant decrease of the water content was found to occur in the first part of the secondary drying, particularly during the heating ramp of the fluid temperature, the first hours of drying were actually the most relevant to perform the fitting.

As for the previous method, the trend of C_s had to be extracted from NIR spectra (step 1-2), and that corresponding to the initial part of drying was selected for fitting. The MATLAB function *fminsearch* was adopted to look for the best fitting between the experimental values of C_s and the calculated values. The latter was obtained by solving the system of equations (1) and (2) with the MATLAB solver for differential equations *ode15s*, which implemented, at each iteration, an optimized value of E_a and $k_0 a$.

This methodology was applied to runs A3 and B1, estimating the kinetic parameters for sucrose and sucrose-arginine, respectively. For fitting purposes, the runs with the highest product temperature were selected (40°C and 45°C respectively) in order to get the largest variation of product temperature, and, thus, of the drying rate. In this way the desorption kinetics was studied over a larger range of temperature and, thus, the kinetic parameters estimated could be suitable to model the desorption process over a larger set of operating conditions.

For validation purposes, the kinetic parameters estimated from run A3 were used to calculate

the trend of C_s in runs A1, A2 and A4, and compared with the trends obtained experimentally from NIRS. The same validation procedure was done with the kinetic parameters estimated for run B1, comparing the calculated C_s with the experimental trend of B2.

2.5 Design space calculation

Once the kinetic parameters are known, they can be used to build a design space to optimize the secondary drying. The detailed procedure to calculate a design space was described step by step by Pisano et al.[28]. The design space can be used to determine the drying time (t_d) required to get the target residual moisture ($C_{s,t}$).

Some constraints regarding the maximum allowed product temperature can be added to the design space. This requires to know the glass transition temperature of the product (T_g) as a function of the water content, as a higher C_s reduces T_g. The simplified Gordon-Taylor equation[59] may be adopted to estimate the T_g:

$$T_g = \frac{C_s\,T_{g,w} + K(1 - C_s)T_{g,s}}{C_s + K(1 - C_s)} \tag{5}$$

where $T_{g,w}$ and $T_{g,s}$ are the glass transition temperature of water and of the solute, and K is a constant taking into account the ratio of the free volumes of the components. A simplified equation[59] to calculate K from the density of the two components (ρ_w and ρ_s) is the following:

$$K = \frac{\rho_w\,T_{g,w}}{\rho_s\,T_{g,s}} \tag{6}$$

To take into account that product B is a mixture of two solutes, the values of $T_{g,s}$ and ρ_s were calculated as the mean of the values of sucrose and of arginine, weighted by their solid fraction. For water and sucrose the values reported by Hancock and Zografi were used[59], while for arginine density was equal to $1.42 \cdot 10^{-3}$ kg m^{-3} [60] and the glass transition temperature to 349 K. The latter was estimated from its melting point, accordingly to Fukuoka et al.[61]. Finally, in order to calculate T_g, the trend of C_s can be obtained from NIRS in-line measurements, or calculated by the model presented above, once all the parameters have been estimated.

Once T_g is estimated for a specific trend of C_s, the corresponding value of the fluid temperature ($T_{f,max}$) that would cause a product temperature equal to the maximum one can be obtained from equation (1) using T_g instead of T_P, and plotted over the design space. The entire profile

of T_P was taken to calculate T_g, allowing to calculate the design space corresponding also to the first hours of secondary drying. In fact, product temperature typically increases suddenly at the beginning of the secondary drying, due to the fluid temperature ramp, while the water content may be still not very low. For this reason, the initial hours of secondary drying can be critical for product quality, and making use of the design space may be beneficial.

The couple of operating conditions T_f and t_d belongs to the design space if that point stays below $T_{f,max}$, i.e. if the value of T_P is lower than the limit value, which is lastly the Quality-by-Design concept. Once the design space is known, the optimal operating conditions may be easily identified by looking for the values of shelf temperature that allows minimizing the duration of this stage, being the duration readily available in the diagram.

3. Results and Discussion

3.1 Kinetic parameters estimation using method #1

The runs A1, A2, A3 at three different temperatures were used to build an Arrhenius plot and get the kinetic parameters for sucrose. The time range 5 h - 20 h was selected, as here the product temperature was almost constant and a quite significant decrease of C_s could still be found. Arrow a points out the range selected in Figure 1 (above).

For each run, r_d was calculated from the smoothed profile of C_s, as described in the procedure above at point 4, and plotted against the driving force of the desorption, according to equation (3). In Figure 1 (below) the linear dependence of r_d on C_s can be inferred, proving the suitability of a linear equation like equation (3) to describe the desorption phenomena. The slope of the fitting lines was used to get the values of the kinetic constants (k_0a), represented in the Arrhenius plot in Figure 2. Here, the linear regression resulted in a very accurate fitting of the three values of k_0a (R^2 equal to about 0.96), underlining the suitability of equation (4) for describing the desorption process. From the interpolation of data in the Arrhenius plot, k_0a and E_a resulted equal to about 245 s^{-1} and 37.27 kJ mol^{-1}.

These values were used to validate the model and the comparison between the trend of C_s predicted by the model and obtained from NIRS measurements can be appreciated in Figure 3. The fitting between the experimental and the calculated values of C_s resulted in low values of RMSE, ranging between 0.105 and 0.274 (Table 2), pointing out the goodness of the algorithm. The model, using the kinetic parameters estimated, allowed to calculate fairly accurate values of C_s both at the beginning of the secondary drying stage, where moisture decrease is much

more relevant, and the stationary value of C_s reached in the last hours of drying, that represent one of the most important final product quality attributes.

3.2 Kinetic parameters estimation using method #2

3.2.1 Product A

As it was pointed out, the most significant decrease of the water content occurred in the first hours of drying: in this case study, by the 6th hour of secondary drying, the decrease of water content ranged between the 77% and the 90% of the entire water content decrease occurring in the secondary drying. Therefore, data in the time range up to 6 h were taken for estimating the kinetic parameters using method #2. Arrow b in Figure 1 (above) points to the range selected. The trend of C_s of run A3 was used, as it was performed at the highest temperature between the runs performed with product A.

The values of k_0a and E_a, found to give the best fitting, were equal to about 213 s^{-1} and 36.92 kJ mol^{-1}. These were very similar to what obtained from the previous procedure, thus the two couples of kinetic parameters confirm the values of each other. Moreover, these values are in good agreement with what Pisano et al. (2012)[28] found for a similar product, i.e. freeze-dried solution of sucrose 5% (w/w), being in that case the kinetic parameters equal to 277 s^{-1} and 37.71 kJ mol^{-1}. Figure 4 shows the validation of the optimized kinetic parameters used for predicting the trend of C_s of run A1, A2, and A4, as well as the remaining hours of run A3. Being similar to the previous values of k_0a and E_a, the comparison between the experimental and the calculated trend of C_s was again very accurate, both in the initial transient, and in the final steady-state values. Also the values of RMSE were found almost equal to the values calculated using method #1, or slightly lower. The values of RMSE for each run of product A could be seen in Table 2, pointing out that method #2 was as much performing and accurate than method #1.

3.2.2 Product B

In order to validate the method with another product, the method #2 was applied to sample B. The run B1, performed at higher temperature, was considered in this framework. As for product A, data in the time range up to 6 h from the beginning of secondary drying were taken, as the decrease of water content in these hours was calculated to range between the 79% and the 96% of the total decrease of water content during the secondary drying. The optimized k_0a and E_a for product B were found equal to about 8 s^{-1} and 27.39 kJ mol^{-1}, which were used to perform

the comparison between the experimental and the calculated trends of C_s. Figure 5 highlight the agreement between the two trends, both for run B2 and for the hours of drying of run B1 not used for the fitting operations. As in paragraph 3.2.1, some aspects of the fitting are remarkable and have to be underlined. Firstly, the overall accuracy in predicting the trend of C_s in all its parts, both at the beginning and at the end of the secondary drying stage, being the last values of C_s equivalent to the RM content in the final product. Also, the kinetic parameters were suitable to model test B2, used exclusively for validation purposes, as well as the second part of B1, not used for best fitting. In fact, the fitting between the experimental and calculated values of C_s resulted in very low values of RMSE, underlining the accuracy of method #2 and its suitability for being applied to different products. If compared to the parameters obtained for product A, it appears that the pre-exponential factor is lower, but also the activation energy is lower, about 30%, that motivates the faster drying kinetics that may be pointed out when comparing the trends in Figure 5 and 4 for the two products.

3.3 Design space calculation

Once the model and the kinetic parameters were obtained and validated, they were used to calculate the design space of product B. The maximum product temperature was calculated using equations (5) and (6), adapted for the mixture of sucrose - arginine. Some parameters were changed, e.g. $C_{s,0}$ and the heating rate, to investigate their effect on the design space.

Figure 6(a) and 6(b) show the design space calculated considering the same heating rate but a different $C_{s,0}$, equal to 6% and 4% respectively. The dashed line represents $T_{f,max}$, i.e. the boundary operating conditions that would cause a product temperature equal to the maximum allowed one. The curves reported are parametrized according to the target residual moisture. For a lower $C_{s,t}$, the drying time increases, e.g. in Figure 6(a) about 4.7 h and 7.2 h to get $C_{s,t}$ equal to 1% and 0.5% with T_f sets at 30°C.

Not surprisingly, when $C_{s,0}$ is higher, a longer drying time is needed (about 10.7 h to get $C_{s,t}$ equal to 0.5% setting T_f at 20°C in Figure 6(a), and 9.5 h in Figure 6(b) in case the residual amount of water at the beginning of secondary drying moves from 6% to 4%). In any case, it has to be remarked that even if the value of $C_{s,0}$ is decreased by one third, the time required to get the target value of residual moisture in the final product is decreased only of about 9%. On the other hand, the hours of primary drying to be performed to lower the value of $C_{s,0}$ may be much longer. Therefore, applying an over-extended primary drying and a shorter secondary drying to get a certain $C_{s,t}$ may be not always the best choice. However, it must be considered that, during the first hours of drying, in case of a higher $C_{s,0}$, the constraint on the T_g is more

stringent. In fact, in Figure 6(a) $T_{f,max}$ at the beginning is about 20°C, while it is more than 10°C higher in Figure 6(b). Consequently, a lower heating rate seems advisable in case of higher $C_{s,0}$. Another observation to be underlined is about the minimum value of $C_{s,t}$ obtainable. Since the desorption kinetic is influenced by the equilibrium value of RM, and $C_{s,eq}$ reaches lower values as the product temperature decreases, some very low values of $C_{s,t}$ could not be obtained with lower fluid temperature. For example, a residual moisture of 0.3% is obtained only if T_f is set to a value higher than 35°C.

Figure 7(a) shows an example of design space for the secondary drying calculated for $C_{s,0}$ equal to 5% and a heating rate of +1°C/min. Figure 7(b), similarly to Figure 7(a), shows the design space for a sample of product B with $C_{s,0}$ equal to 5% but dried with a higher heating rate. Obviously, the higher the target residual moisture, the lower is t_d: at T_f equal to 20°C, $C_{s,t}$ of 2% and of 1% are reached respectively, in Figure 7(a), in about 5.3 h and 8.0 h, and, in Figure 7(a), in about 3.3 h and 6.0 h. This also means that a shorter drying time may be a consequence of a higher heating rate. In fact, with a higher heating rate, the set point value of T_f is reached quicker, and the drying is performed to a higher temperature since early.

It is also interesting to notice that the lower the heating rate, the less relevant is the set point value of T_f. Indeed, from a comparison of the curves at $C_{s,t}$ equal to 2% in Figure 7(a) and 7(b), it appears as a vertical line, meaning that the target residual moisture is reached at the same time regardless the set point T_f. This is reasonable as, from the experimental trends (Figures S2 and S4 in Supplementary material), a major part of the decrease of the water content was observed, actually, during the fluid temperature ramp. Therefore, the fact that with a lower heating rate the T_f is not relevant to shorten t_d, just means that $C_{s,t}$ is reached while the fluid temperature is still being increased, i.e. is reached before T_f arrives at the set point value. The fact that in both Figure 6(a) and 6(b) the curves corresponding to a higher target residual moisture ($C_{s,t}$ equal to 3%) are basically not affected by T_f is just another aspect of what just explained: $C_{s,t}$ is close to $C_{s,0}$ and the decrease of the water content to get $C_{s,t}$ can be performed entirely during the first part of the heating rate.

A last consideration can be done about how $C_{s,0}$ and the heating rate may affect the boundary operating conditions, i.e. the value of the glass transition temperature. Comparing the design spaces in Figure 6, it appeared that the constraint on the T_g is stronger in case of a higher $C_{s,0}$. Considering, for example, the curve at $C_{s,t}$ equal to 2% and 0.5%, the corresponding $T_{f,max}$ are about 38°C and 46°C if $C_{s,0}$ is equal to 4% (Figure 6(b)), and about 36°C and 44°C if $C_{s,0}$ is equal to 6% (Figure 6(a)). Actually, this may be a consequence of T_g being affected by C_s, i.e. an higher amount of water content makes the maximum product temperature lower. Concerning

the heating rate effect, during the fluid temperature ramp in the first hours of secondary drying, it seemed that a lower heating rate would allow higher fluid temperature. For example, the T_f associated to $C_{s,t}$ equal to 2% and to 0.3% is respectively about 42°C and 50°C for a heating rate of +1°C/min (Figure 7(a)), but it is decreased to 36°C and 48°C for a higher heating rate (Figure 7(b)). This can still be due to the relationship between the water content and T_g. If the fluid temperature is increased quickly, a higher product temperature is reached sooner than a significant decrease of C_s, i.e. T_P reaches a higher value when C_s is still not low enough to allow that temperature. In this case, to avoid T_P exceeding T_g a lower value of T_f should be set.

4. Conclusions

In this work NIRS was used as an in-line tool for freeze-drying monitoring, in order to measure the water content in a vial during the secondary drying. The information provided by NIRS were used to estimate the kinetic parameters of the water desorption reaction, suitable for describing *in silico* the secondary drying. Two methodologies were presented to estimate the kinetic parameters, and both were validated. It has to be underlined that method #2 requires a single test, and just measurements in the first part of the process are used. This allowed to estimate in-line (i) the drying time required to get a target residual moisture and (ii) the design space, thus pointing out if the heating temperature has to be changed and which is the effect of this change.

Although in-line application of NIRS is feasible, even in industrial-scale apparatus, and, thus, the proposed approach could be used for in-line development of the design space of the secondary drying stage, due to the low computational time, our suggestion is to use it in the stage of process development, carried out at lab-scale, where surely the installation of NIRS is less problematic.

An intrinsic limitation of this approach is related to the fact that the NIRS probe tracks the residual moisture in just one of the vials of the batch. In this framework it has to be highlighted that in the proposed set-up we are measuring not only the desorption rate in one vial, but also its temperature (actually, the temperature in a vial close to that monitored through NIRS, but we may assume the temperature difference being negligible). Therefore, what we get are the kinetic parameters of the desorption process for the specific product being processed. Obviously a certain uncertainty about these parameters may exist, and this could be accounted for as for the design space calculation of the primary drying stage. This uncertainty may be evaluated in-

line by using several probes, thus monitoring more than one vials: this could be surely done at least at lab scale.

As the vial monitored by NIRS could be considered an edge vial, it has to be taken into account that a design space derived with this approach would be referred to edge vials. By simply considering the K_v of central vials all calculations may be repeated for the other group of vials. Finally, the effect of different process conditions on the design space were investigated. Obviously, the higher the water content at the beginning of secondary drying, the longer the drying time required to reach the target residual moisture. However, the drying time saved in case $C_{s,0}$ was lower might be not so advantageous as a much longer primary drying should be performed to lower $C_{s,0}$. Concerning the heating rate, when it was higher the maximum allowed product temperature appeared to decrease, as a consequence of being the water content decrease slower than the product temperature increase. Therefore, for more heat-sensitive products a lower heating rate would be advisable.

Finally, it has to be remarked that in the present study we considered that secondary drying is carried at constant temperature, as it is generally done in industrial environment. Obviously, once a validated mathematical model is available, and also the kinetic parameters for the desorption reaction in the system under investigation are known, it is possible to analyze the effect of modifying the heating fluid temperature, thus carrying out the secondary drying in two or more steps. This will add a degree of freedom to the analysis, making impossible to obtain a simple graphical representations of the design space of the secondary drying, but it could allow shortening the duration of this step, in particular when the resulting drying time is considered unacceptable for the industrial manufacturing.

References

[1] https://www.fda.gov/regulatory-information/search-fda-guidance-documents/pat-framework-innovative-pharmaceutical-development-manufacturing-and-quality-assurance

[2] Fissore, D.; McCoy, T. Editorial: freeze-drying and process analytical technology for pharmaceuticals, *Front. Chem.* **2018**, 6, 1-2. DOI: 10.3389/fchem.2018.00622.

[3] Tang, X., Pikal M.J., Design of freeze-drying processes for pharmaceuticals: practical advice. *Pharm. Res*. **2004**, 21, 191-200. DOI: 10.1023/B:PHAM.0000016234.73023.75.

[4] Patel, S. M.; Doen, T. Pikal, M. J.; Determination of end point of primary drying in freeze-drying process control. *AAPS PharmSciTech*. **2010**, 11, 73-84. DOI: 10.1208/s12249-009-9362-7.

[5] Roy, M. L.; Pikal, M. J. Process control in freeze drying: determination of the end point of sublimation drying by an electronic moisture sensor. *PDA J Pharm Sci Technol*. **1989**, 43, 60-66.

[6] Pisano, R. Automatic control of a freeze-drying process: detection of the end point of primary drying. *Drying Technol*. **2020.** DOI: 10.1080/07373937.2020.1774891.

[7] Liapis, A. I.; Bruttini, R. A theory for the primary and secondary drying stages of the freeze-drying of pharmaceutical crystalline and amorphous solutes: comparison between experimental data and theory. *Sep. Technol.* **1994**, 4, 144-155. DOI: 10.1016/0956-9618(94)80017-0.

[8] Hottot, A.; Peczalski, R.; Vessot, S.; Andrieu, J. Freeze-Drying of pharmaceutical proteins in vials: modeling of freezing and sublimation steps. *Drying Technol*. **2006**, 24, 561-570. DOI: 10.1080/07373930600626388.

[9] Velardi, S. A.; Barresi, A. A. Development of simplified models for the freeze-drying process and investigation of the optimal operating conditions. *Chem. Eng. Res. Des*. **2008**, 86, 9–22. DOI: 10.1016/j.

[10] Fissore, D.; Barresi, A. A. Scale-up and Process Transfer of Freeze-Drying Recipes. *Drying Technol*. **201**1, 29, 1673-1864, DOI: 10.1080/07373937.2011.597059.

[11] Fissore, D.; Pisano, R.; Barresi, A. A. Using mathematical modeling and prior knowledge for qbd in freeze-drying processes. In: *Quality by Design for Biopharmaceutical Drug Product Development*, Jameel, F., Eds.; Springer Science: New York, **2015**; pp 565–593.

[12] Giordano, A.; Barresi, A. A.; Fissore, D. On the use of mathematical models to build the design space for the primary drying phase of a pharmaceutical lyophilization process. *J. Pharm. Sci*. **2011**, 100, 312-324. DOI: 10.100[2/jps.22264

[13] Kodama, T.; Takeuchi, M.; Wakiyama, N.; Terada, K. Optimization of secondary drying condition for desired residual water content in a lyophilized product using a novel simulation program for pharmaceutical lyophilization. *Int. J. Pharm*. **2014**, 469, 59-66, DOI: 10.1016/j.ijpharm.2014.04.043.

[14] Sadikoglu, H.; Liapis, A.I.; Crosse, O.K. Optimal control of the primary and secondary drying stages of bulk solution freeze drying in trays. *Drying Technology*. **1998**, 16, 399-431. DOI: 10.1080/07373939808917417.

[15] Stratta, L.; Capozzi, L. C.; Franzino, S.; Pisano, R. Economic analysis of a freeze-drying cycle. *Processes.* **2020**, 8, 1399-1416. DOI: 10.3390/pr8111399.

[16] De Beer, T.; Vercruysse, P.; Burggraeve, A.; Quinten, T.; Ouyang, J.; Zhang, X.; Vervaet, C.; Remon, J. P.; Baeyens, W. R.G. In-line and real-time process monitoring of a freeze drying process using Raman and NIR spectroscopy as complementary process analytical technology (PAT) tools. *J. Pharm. Sci*. **2009**, 98, 3430-3446. DOI: 10.1002/jps.21633.

[17] Fissore, F.; Pisano, P.; Barresi, A.A. Process analytical technology for monitoring pharmaceuticals freeze-drying – A comprehensive review. *Drying Technol*. **2018**, 36, 1839-1865**.** DOI: 10.1080/07373937.2018.1440590.

[18] Fissore, D.; Pisano, R. Computer-aided framework for the design of freeze-drying cycles: optimization of the operating conditions of the primary drying stage. *Processes*. **2015**, 3, 406-421. DOI: 10.3390/pr3020406.

[19] Trelea, I. C.; Fonseca, F.; Passot, S. Dynamic modeling of the secondary drying stage of freeze drying reveals distinct desorption kinetics for bound water. *Drying Technol*. **2016**, 34, 335–345. DOI: 10.1080/07373937.2015.1054509.

[20] Oddone, I.; Barresi, A. A.; Pisano, R. Influence of controlled ice nucleation on the freeze-drying of pharmaceutical products: the secondary drying step. *Int. J. Pharm*. **2017**, 524, 134–140. DOI: 10.1016/j.ijpharm.2017.03.077.

[21] Pikal, M. J.; Shah, S.; Roy, M. L.; Putman, R. The secondary drying stage of freeze drying: drying kinetics as a function of temperature and chamber pressure, *Int. J. Pharm*. **1990**, 60, 203-217. DOI: 10.1016/0378-5173(90)90074-E.

[22] Searles, J. A.; Aravapalli, S.; Hodge, C. Effects of chamber pressure and partial pressure of water vapor on secondary drying in lyophilization. *AAPS PharmSciTech.* **2017**, 18, 2808–2813. DOI: 10.1208/s12249-017-0768-3.

[23] Assegehegn, G.; Brito-de la Fuente, E.; Franco, J. M.; Gallegos, C. Understanding and optimization of the secondary drying step of a freeze-drying process: a case study. *Drying Technol*. **2021**, 9, 1003-1017,. DOI: 10.1080/07373937.2020.1739065.

[24] Pikal, M. J.; Tang, X. C.; Nail, S. L. Automated process control using manometric temperature measurement. U. S. patent US 6971187 B1, **2005**.

[25] Mayeresse, Y. Moisture content in freeze-dried product. Cambridge Healthtech Institute's Seventh Annual Pep Talk 2008, San Diego, California, January 7–11, **2008**.

[24] Schneid, S.; Gieseler, H. Process analytical technology (PAT) in freeze-drying: Tunable Diode Laser Absorption spectroscopy as an evolving tool for cycle monitoring. *Eur Pharm Rev*. **2009**, 6, 18-25.

[27] Fissore, D.; Pisano, R.; Barresi, A. A.; Monitoring of the secondary drying in freeze-drying of pharmaceuticals. *J. Pharm. Sci*. **2011**, 100, 732-742. DOI: 10.1002/jps.22311.

[28] Pisano, R.; Fissore, D.; Barresi, A. A. Quality by Design in the secondary drying step of a freeze-drying process. *Drying Technol*. **2012**, 30, 1307-1316, DOI: 10.1080/07373937.2012.704466.

[29] Luypaert, J.; Massart, D. L.; Vander Heyden, Y. Near-infrared spectroscopy applications in pharmaceutical analysis. *Talanta*. **2007**, 7, 865-883. DOI: 10.1016/j.talanta.2006.12.023.

[30] Ciurczak, E. W.; Drennen, J. K.; Pharmaceutical and medical applications of near-infrared spectroscopy, Marcel Dekker, New York, **2002**.

[31] Blanco, M.; Coello, J.; Iturriaga, H.; Maspoch, S.; De La Pezuela, C. Near-infrared spectroscopy in the pharmaceutical industry. *Analyst*. **1998**, 123, 135R-150R. DOI: 10.1039/A802531B.

[32] Osborne, B. G. Near-infrared spectroscopy in food analysis. In: *Encyclopedia of Analytical Chemistry*, Meyer, R. A., Ed.; John Wiley & Sons: New York, **2006**.

[33] Pasquini, C. Near infrared spectroscopy: a mature analytical technique with new perspectives - A review. *Anal. Chim. Acta*. **2018**, 1026, 8-36. DOI: 10.1016/j.aca.2018.04.004.

[34] Zheng, Y.; Lai, X.; Bruun, S. W.; Ipsen, H.; Larsen, J. N.; Løwenstein, H.; Søndergaard, I.; Jacobsen, S. Determination of moisture content of lyophilized allergen vaccines by NIR spectroscopy. *J. Pharmaceut. Biomed*. **2008**, 46, 592-596. DOI: 10.1016/j.jpba.2007.11.011.

[35] Jones, J. A.; Last, I. R.; Macdonald, B. F.; Prebblet, K. A. Development and transferability of near-infrared methods for determination of moisture in a freeze-dried injection product. *J. Pharmaceut. Biomed*. **1993**, 11, 1227-1231. DOI: 10.1016/0731-7085(93)80108-D.

[36] Li, Y.; Fan, Q.; Liu, S.; Wang, L. Simultaneous analysis of moisture, active component and cake structure of lyophilized powder for injection with diffuse reflectance FT-NIR chemometrics. *J. Pharmaceut. Biomed*. **2011**, 55, 216-219. DOI: 10.1016/j.jpba.2010.12.028.

[37] Last, I. R.; Prebble, K.A. Suitability of near-infrared methods for the determination of moisture in a freeze-dried injection product containing different amounts of the active ingredient. *J. Pharmaceut. Biomed*. **1993**, 11, 1071-1076, DOI: 10.1016/0731-7085(93)80084-E.

[38] Derksen, M. W. J.; van der Oetelaarb, P. J. M.; Maris, F. A. The use of near-infrared spectroscopy in the efficient prediction of a specification for the residual moisture content of a freeze-dried product. *J. Pharmaceut. Biomed*., **1998**, 17, 473-480. DOI: 10.1016/S0731-7085(97)00216-1.

[39] Clavaud, M.; Roggo, Y.; Degardin, K.; Sacre, P.-Y.; Hubert, P.; Ziemons, E. Moisture content determination in an antibody-drug conjugate freeze-dried medicine by near-infrared spectroscopy: a case study for release testing. *J. Pharm. Biomed. Anal*. **2016**, 131, 380-390. DOI: 10.1016/j.jpba.2016.09.014.

[40] De Beer, T.; Burggraeve, A.; Fonteyne, M.; Saerens, S.; Remon, J. P.; Vervaet, C. Near infrared and Raman spectroscopy for the in-process monitoring of pharmaceutical production processes. *Int. J. Pharm*. **2011**, 417, 32-47. DOI: 10.1016/j.ijpharm.2010.12.012.

[41] Pieters, S.; De Beer, T.; Kasper, J. C.; Boulpaep, D.; Waszkiewicz, O.; Goodarzi, M.; Tistaert, C.; Friess, W.; Remon, J.; Vervaet, C.; Vander Heyden, Y. Near-Infrared spectroscopy for in-line monitoring of protein unfolding and its interactions with lyoprotectants during freeze-drying. *Anal. Chem.* **2012**, 84, 947-955. DOI: 10.1021/ac2022184.

[42] Rosasa, J. G.; Waard, H.; De Beerd, T.; Vervaet, C.; Remonc, J. P.; Hinrichs, W. L. J.; Frijlink, H. W.; Blanco, M. NIR spectroscopy for the in-line monitoring of a multicomponent formulation during the entire freeze-drying process. *J. Pharmaceut. Biomed.* **2014**, 97, 39-46. DOI: 10.1016/j.jpba.2014.04.010.

[43] Mensink, M. A.; Van Bockstal, P.; Pieters, S.; De Myer, L.; Frijlink, H. V.; van der Voort Maarschalk, K.; Hinrichs, W. L. J.; De Beer, T. In-line near infrared spectroscopy during freeze-drying as a tool to measure efficiency of hydrogen bond formation between protein and sugar, predictive of protein storage stability. *Int. J. Pharmaceut.* **2015**, 496, 792-800. DOI: 10.1016/j.ijpharm.2015.11.030.

[44] De Beer, T.; Wiggenhorn, M.; Veillon, R.; Debacq, C.; Mayeresse, Y.; Moreau, B.; Burggraeve, A.; Quinten, T.; Friess, W.; Winter, G.; Vervaet, C.; Remon, J. P.; Baeyens, W. R. G. Importance of using complementary process analyzers for the process monitoring, analysis, and understanding of freeze drying. *Anal. Chem.* **2009**, 81, 7639-7649. DOI: 10.1021/ac9010414.

[45] Kauppinen, A.; Toiviainen, M.; Korhonen, O.; Aaltonen, J.; Järvinen, K.; Paaso, J.; Juuti, M.; Ketolainen, J. In-line multipoint near-infrared spectroscopy for moisture content quantification during freeze-drying. *Anal. Chem.* **2013**, 85, 2377−2384. DOI: 10.1021/ac303403p.

[46] Bobba, S.; Zinfollino, N.; Fissore, D. On the development of a robust model for the determination of the residual moisture in freeze-dried products using Near-Infrared Spectroscopy. *J. Pharm. Sci.*, DOI: 10.1016/j.xphs.2021.10.015.

[47] Reich, G. Near-infrared spectroscopy and imaging: basic principles and pharmaceutical applications. *Adv Drug Deliver Rev.* **2005**, 57, 1109-1143. DOI: 10.1016/j.addr.2005.01.020.

[48] Roggo, Y.; Chalus, P.; Maurer. L.; Lema-Martinez, C.; Edmond, A.; Jent, N. A review of near infrared spectroscopy and chemometrics in pharmaceutical technologies. *J Pharm Biomed Anal.* **2007**, 44, 683-700. DOI: 10.1016/j.jpba.2007.03.023.

[49] Rambhatla, S.; Pikal, M. J. Heat and mass transfer scale-up issues during freeze-drying, I: atypical radiation and the edge vial effect. *AAPS PharmSciTech.* **2003**, 4, 1-10. DOI: 10.1208/pt040214.

[50] Rambhatla, S.; Tchessalov, S.; Pikal, M. J. Heat and mass transfer scale-up issues during freeze-drying, III: control and characterization of dryer differences via operational qualification tests. *AAPS PharmSciTech.* **2006**, 7, E1-E10. DOI: 10.1208/pt070239.

[51] Bobba, S.; Zinfollino, N.; Fissore, D. Application of Near-Infrared Spectroscopy to statistical control in freeze-drying processes. *Eur. J. Pharm. Biopharm.*, **2021**, 168, 26-37. DOI: 10.1016/j.ejpb.2021.08.009.

[52] Ward, H. W.; Sistare, F. E. On-line determination and control of the water content in a continuous conversion reactor using NIR spectroscopy. *Anal. Chim. Acta*, **2007**, 595, 319-322, DOI: 10.1016/j.aca.2007.03.020.

[53] Grohganz, H.; Fonteyne M.; Skibsted, E.; Falck, T.; Palmqvist, B.; Rantanen, J. Role of excipients in the quantification of water in lyophilized mixtures using NIR spectroscopy. *J. Pharm. Biomed. Anal*. **2009**, 49, 901-907, DOI: 10.1016/j.jpba.2009.01.021.

[54] Pikal, M. J.; Roy, M. L.; Shah, S. Mass and heat transfer in vial freeze-drying of pharmaceuticals: role of the vial. *J. Pharm. Sci*. **1984**, 73, 1224-1237. DOI: 10.1002/jps.2600730910.

[55] Pisano, R.; Fissore, D.; Barresi, A. A. Heat transfer in freeze-drying apparatus. In *Developments in Heat Transfer*, Dos Santos Bernardes, M. A., Ed.; InTech: Rijeka, Croatia, **2011**.

[56] Sadikoglu, H.; Liapis, A. I. Mathematical modelling of the primary and secondary drying stages of bulk solution freeze-drying in trays: parameter estimation and model discrimination by comparison of theoretical results with experimental data. *Drying Technol*. **1997**, 15, 791-810. DOI:10.1080/07373939708917262

[57] Pikal, M. J.; Cardon, S.; Bhugra, C.; Jameel, F.; Rambhatla, S. The nonsteady state modeling of freeze drying: in-process product temperature and moisture content mapping and pharmaceutical product quality applications. *Pharm. Dev. Technol*. **2005**, 10, 17-32, DOI: 10.1081/pdt-35869.

[58] Shani, E. K.; Pikal, M. J.; Modeling the secondary drying stage of freeze drying: development and validation of an excel-based model. *J. Pharm. Sci*. **2017**, 106, 779-791. DOI: 10.1016/j.xphs.2016.10.024.

[59] Hancock, B. C.; Zografi, G. The relationship between the glass transition temperature and the water content of amorphous pharmaceutical solids. *Pharm. Res*. **1994**, 11, 471-477. DOI: 10.1023/a:1018941810744.

[60] https://www.chemsrc.com/en/cas/1119-34-2_895095.html, last accessed: 06 July 2021.

[61] Fukuoka, E.; Makita, M.; Yamamura, S. Glassy state of pharmaceuticals. iii. thermal properties and stability of glassy pharmaceuticals and their binary glass systems. *Chem. Pharm. Bull*. **1989**, 37, 1047-1050. DOI: 10.1248/cpb.37.1047.

List of Tables

Table 1. Values of RM (% w/w) measured by KF and predicted by PLS regression applied to NIR spectra, and the experimental values of $C_{s,eq}$.

Table 2. Values of RMSE (%w/w) calculated for each run of product A and B and for method #1 and #2.

List of Figures

Figure 1. Upper graph: evolution of the normalized C_s for product A in the secondary drying stage for different heating fluid temperatures. The arrows indicate the range of data used for estimating the kinetic parameters by interpolation of Arrhenius plot (a), and by optimization (b). Time was set equal to zero at the beginning of the secondary drying. Lower graph: dependence of desorption rate on the driving force of the desorption process for different heating fluid temperatures.
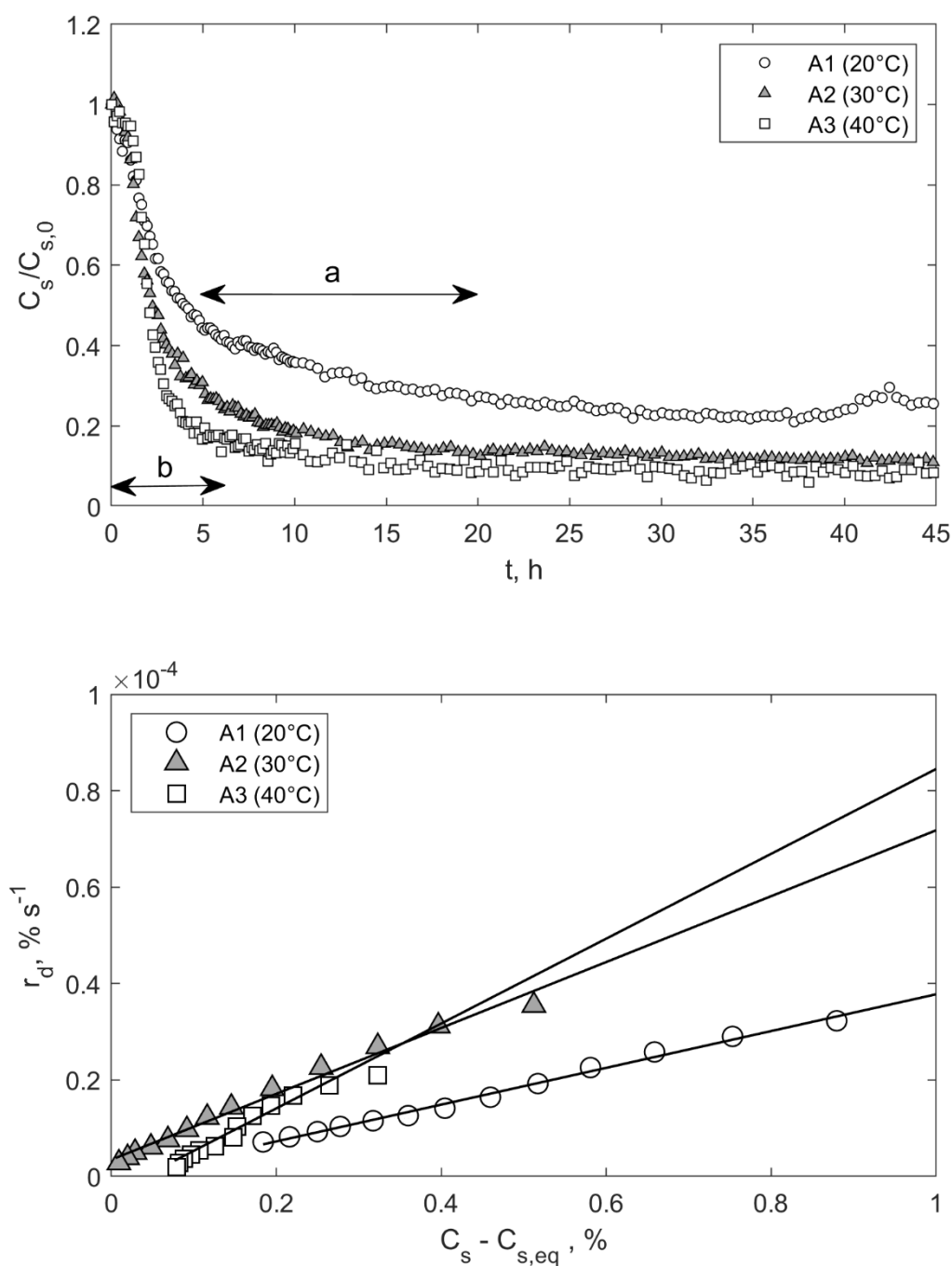
Figure 2. Arrhenius plot for the the desorption process in case of product A.
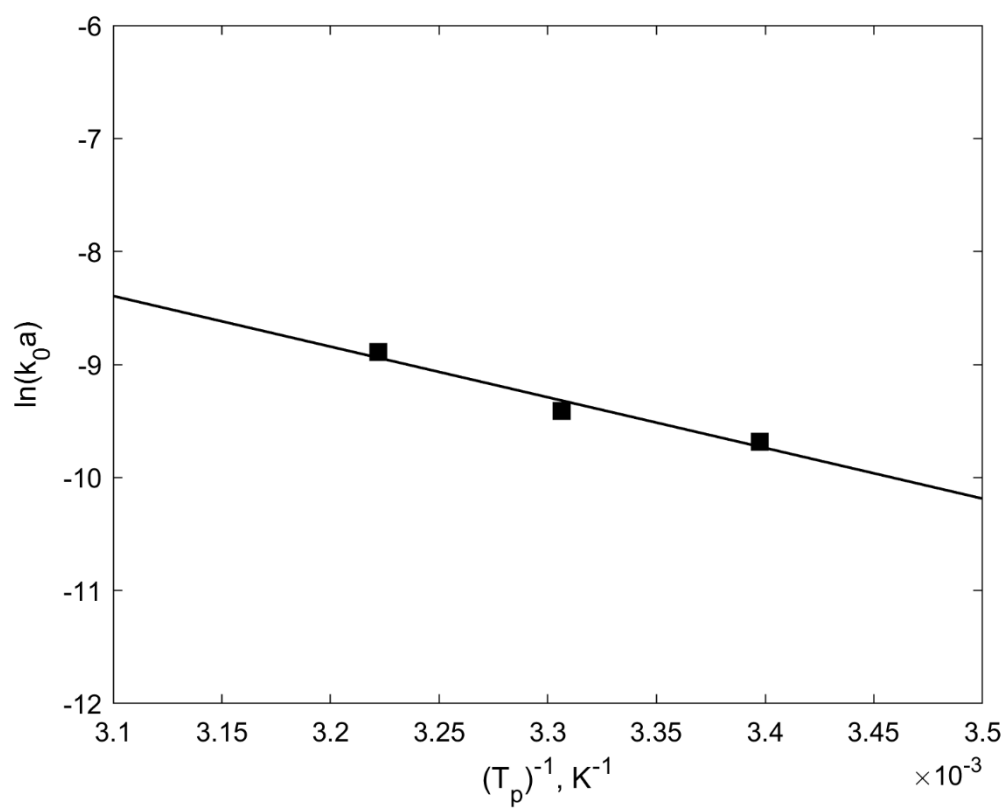
Figure 3. Comparison between the trends of C_s of samples A measured by NIRS (symbols) and predicted by the mathematical model using the kinetic parameters obtained from the Arrhenius plot (solid line). Time was set equal to zero at the beginning of the secondary drying.

Figure 4. Comparison between the trends of C_s of samples A measured by NIRS (symbols) and predicted by the mathematical model using the optimized kinetic parameters obtained from best fitting algorithm (solid line). Time was set equal to zero at the beginning of the secondary drying.

Figure 5. Comparison between the trends of C_s of samples B measured by NIRS (symbols) and predicted by the mathematical model using the optimized kinetic parameters obtained from best fitting algorithm. Time was set equal to zero at the beginning of the secondary drying.

Figure 6. Design space of the secondary drying stage for product B, in case $C_{s,0}$ is equal to 6% (a) and 4% (b). The limit fluid temperature is shown as a function of the drying time. Curves correspond to different $C_{s,t}$, ranging from 0.3% to 3% The dashed line represent the boundary operating conditions to meet the constraint on the T_g of the product.

Figure 7. Design space of the secondary drying stage for product B, in case $C_{s,0}$ is equal to 5% and with different heating rates: +1°C/min (a), and +5°C/min (b). Curves correspond to values of $C_{s,t}$, ranging from 0.3% to 3%. The dashed line represent the boundary operating conditions to meet the constraint on the T_g of the product.

Table 1. Values of RM (% w/w) measured by KF and predicted by PLS regression applied to NIR spectra, and the experimental values of $C_{s,eq}$.

Samples	KF	NIRS	$C_{s,eq}$
A1	0.97	1.01	0.98
A2	0.52	0.57	0.56
A3	0.42	0.35	0.25
A4	0.47	0.37	0.28
B1	0.34	0.33	0.24
B2	0.27	0.24	0.18

Table 2. Values of RMSE (%w/w) calculated for each run of product A and B and for both method #1 and #2.

Run	A1	A2	A3	A4	B1	B2
method #1	0.274	0.222	0.130	0.105	-	-
method #2	0.270	0.221	0.130	0.100	0.112	0.112

Figure 1. Upper graph: evolution of the normalized C_s for product A in the secondary drying stage for different heating fluid temperatures. The arrows indicate the range of data used for estimating the kinetic parameters by interpolation of Arrhenius plot (a), and by optimization (b). Time was set equal to zero at the beginning of the secondary drying. Lower graph: dependence of desorption rate on the driving force of the desorption process for different heating fluid temperatures.

Figure 2. Arrhenius plot for the desorption process in case of product A.

Figure 4. Comparison between the trends of C_s of samples A measured by NIRS (symbols) and predicted by the mathematical model using the optimized kinetic parameters obtained from best fitting algorithm (solid line). Time was set equal to zero at the beginning of the secondary drying.
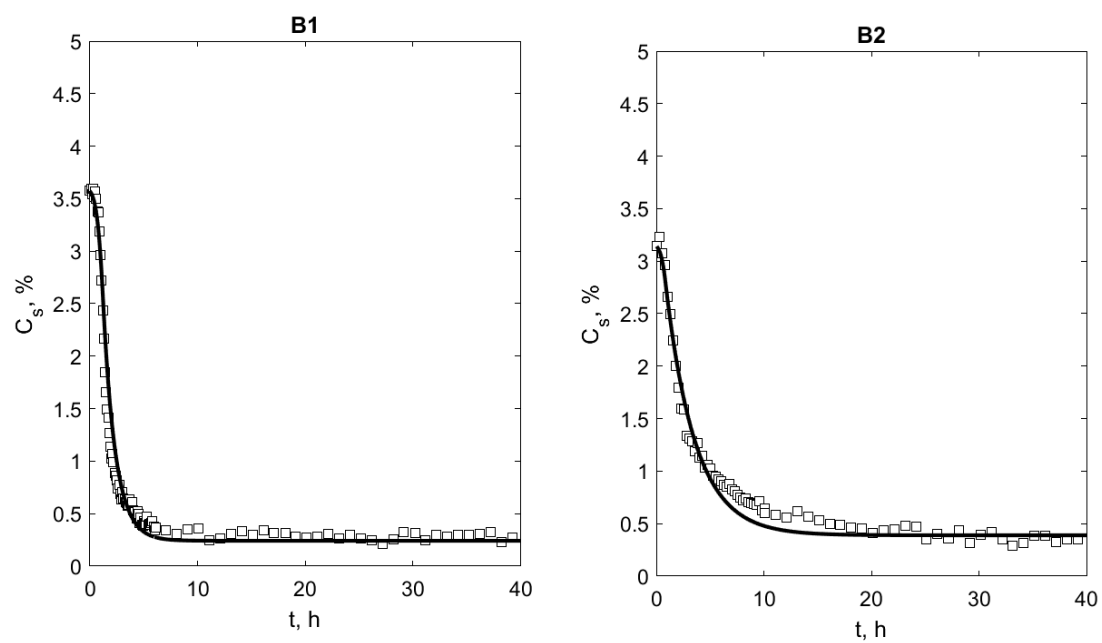
Figure 5. Comparison between the trends of C_s of samples B measured by NIRS (symbols) and predicted by the mathematical model using the optimized kinetic parameters obtained from best fitting algorithm. Time was set equal to zero at the beginning of the secondary drying.

Figure 6. Design space of the secondary drying stage for product B, in case $C_{s,0}$ is equal to 6% (a) and 4% (b). The limit fluid temperature is shown as a function of the drying time. Curves correspond to different $C_{s,t}$ ranging from 0.3% to 3%. The dashed line represent the boundary operating conditions to meet the constraint on the T_g of the product.
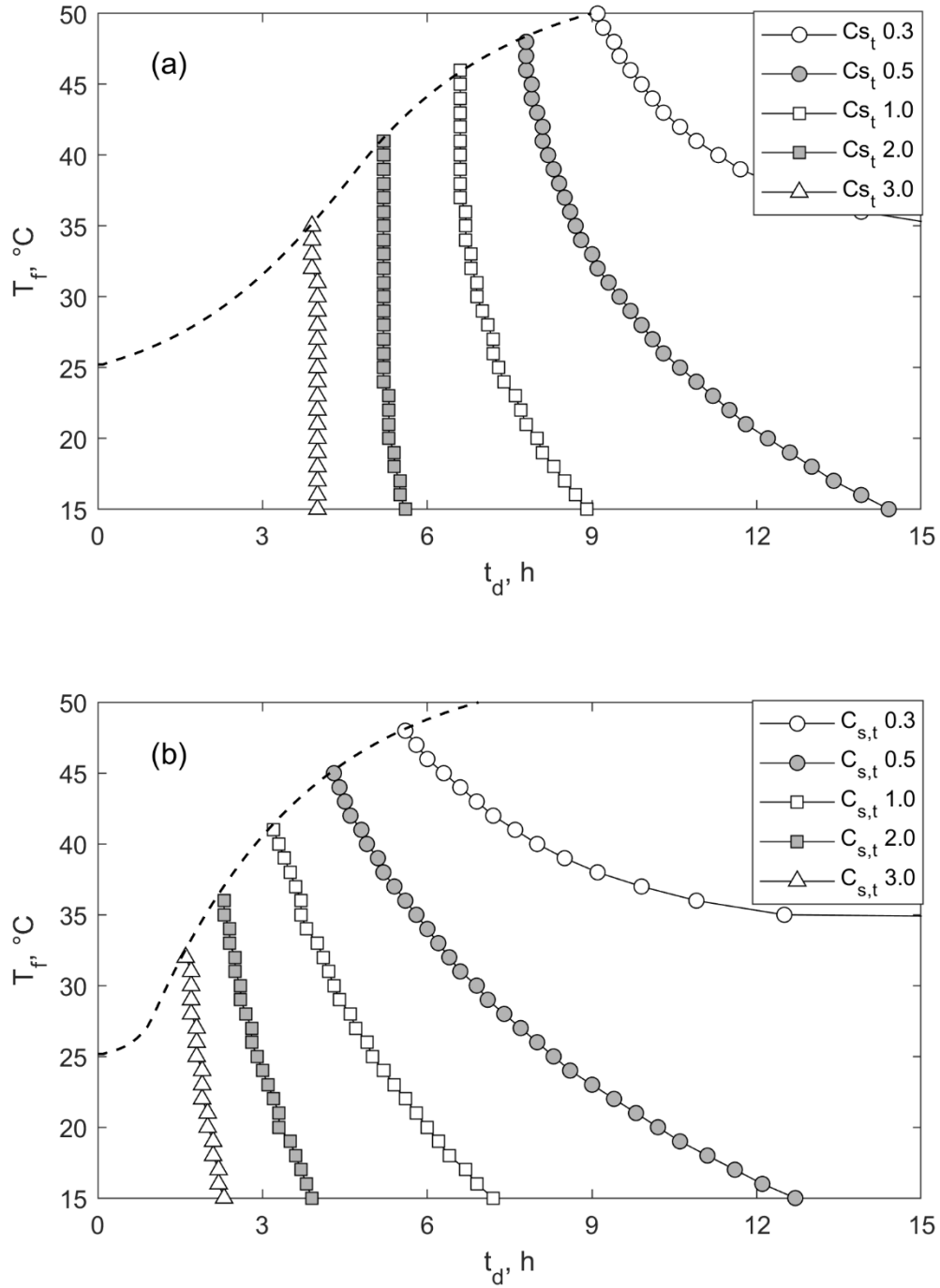
Figure 7. Design space of the secondary drying stage for product B, in case $C_{s,0}$ is equal to 5% and with different heating rates: +1°C/min (a), and +5°C/min (b). Curves correspond to values of $C_{s,t}$, ranging from 0.3% to 3%. The dashed line represent the boundary operating conditions to meet the constraint on the T_g of the product.

Figure S1. Above: Experimental setup for NIRS installation in the freeze-drier chamber and in-line monitoring. Below: Polymeric frame designed for in-line NIRS monitoring of a freeze-drying processes.
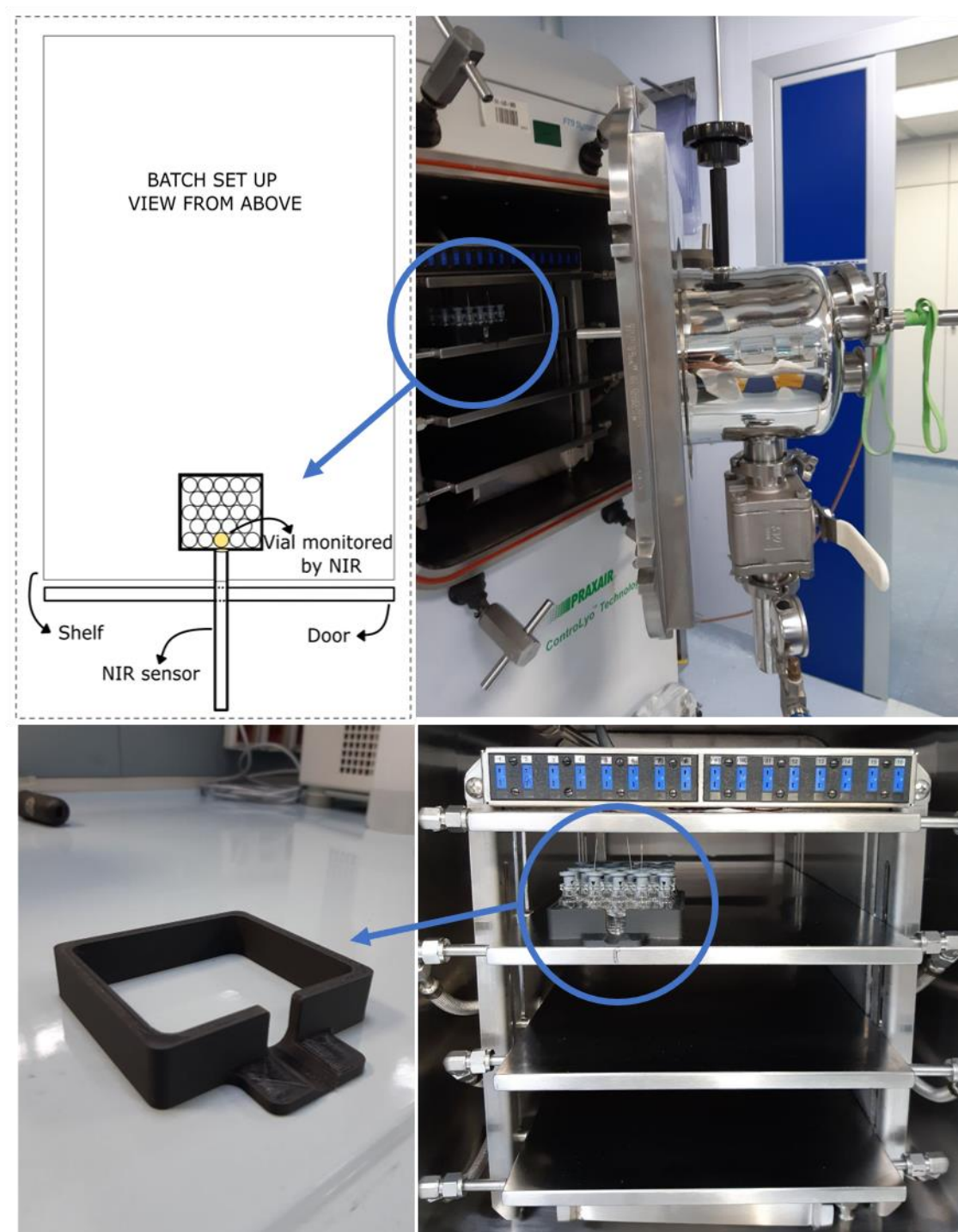
Figure S2. Fluid temperature (upper graph, solid lines), product temperature (upper graph, dashed lines), and water content (C_s) (bottom graph) in the secondary drying stage for the cycles A1 (blue), A2 (orange), A3 (green). Time has been set equal to zero at the beginning of secondary drying.
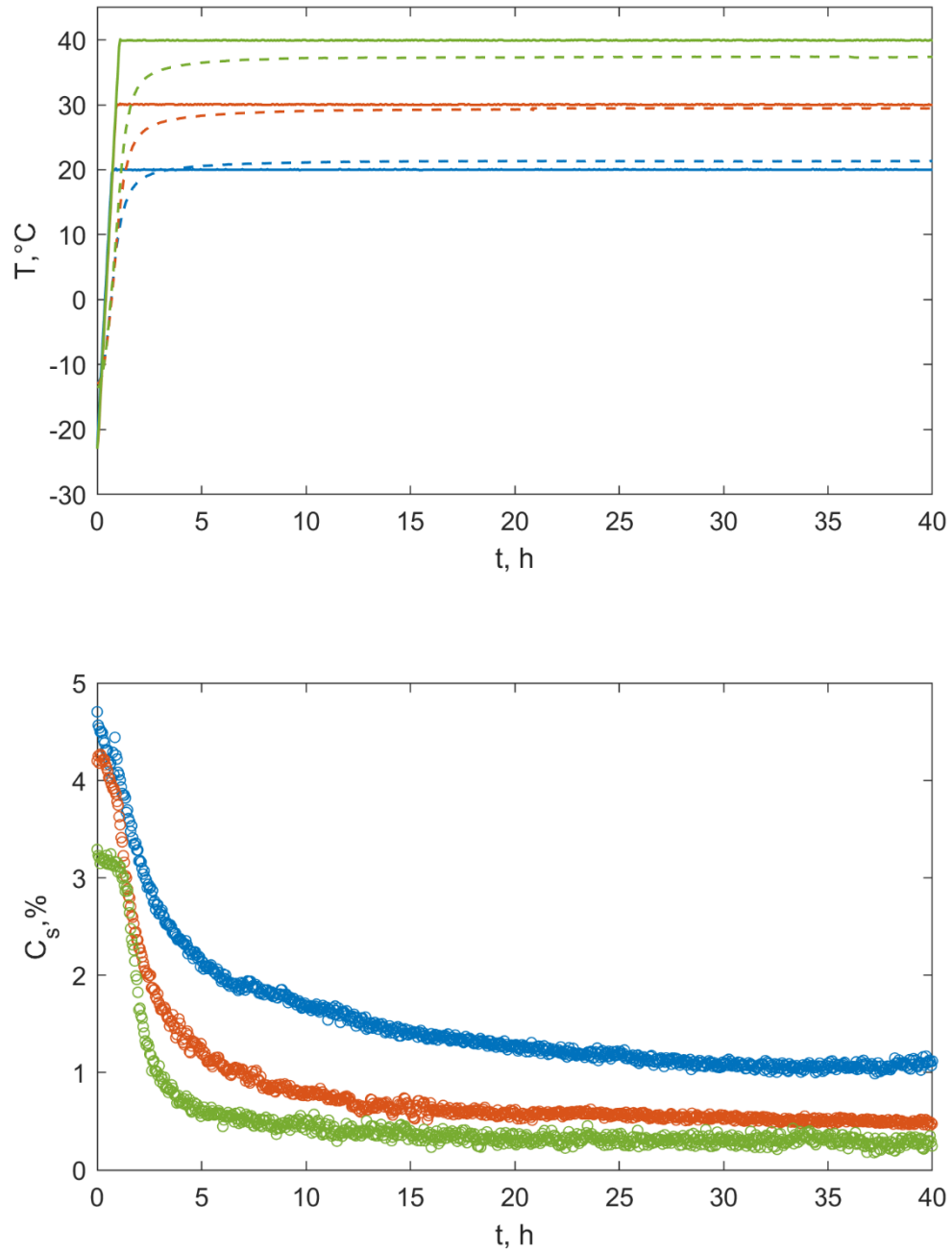
Figure S3. Fluid temperature (upper graph, solid line), product temperature (upper graph, dashed line), and water content (C_s) (bottom graph) in the secondary drying stage of cycle A4.
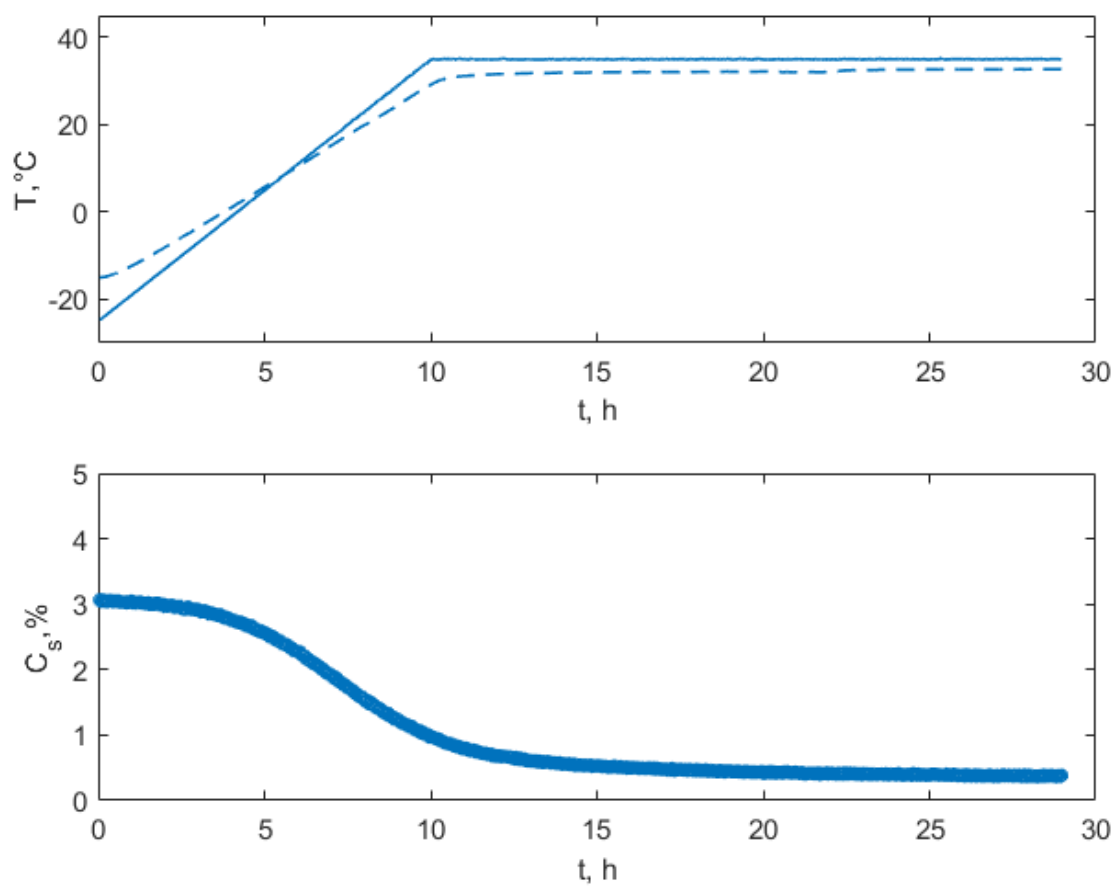
Figure S4. Fluid temperature (upper graph, solid lines), product temperature (upper graph, dashed lines), and water content (C_s) (bottom graph) in the secondary drying stages of cycles B1 (orange) and B2 (blue). Time has been set equal to zero at the beginning of secondary drying.